electron wavefunction and its components reflected on the nearest-neighbour atoms. This interference is destructive or constructive depending on the ratio between the return path length $2r_i$ (where r_i is the radial distance with the ith shell of backscattering atoms) and the wavelength of the excited electron. Fourier analysis of EXELFS structures, from 50 eV above the ionization threshold, gives the radial distribution function around this specific site. This is mostly a technique for measuring the local short-range order. Its accuracy has been established to be better than 0.1 Å on nearest-neighbour distances with test specimens, but such performance requires correction procedures for phase shifts. The method therefore seems more promising for measuring changes in interatomic distances in specimens of the same chemical composition. The major advantage of EXELFS is its applicability for small specimen volumes that can moreover be characterized by other high-resolution electron-microscopy modes. It is also possible to investigate bond lengths in different directions by selecting the scattering angle of the transmitted electron and the specimen orientation (Disko, Krivanek & Rez, 1982). On the other hand, the major limitations of EXELFS are due to the dose requirements for sufficient SNR and to the fact that the accessible excitation range is limited to edges below ~2–3 keV and to oscillation domains ~200 or 300 eV at the maximum.

4.3.4.4.4. *Applications for core-loss spectroscopy*

(*a*) *Quantitative microanalysis*

The main field of application of core-loss EELS spectroscopy has been its use for local chemical analysis (Maher, 1979; Colliex, 1984; Egerton, 1986). The occurrence of an edge superimposed on the regularly decreasing background of an EELS spectrum is an indication of the presence of the associated element within the analysed volume.

Methods have been developed to extract quantitative composition information from these spectra. The basic idea lies in the linear relationship between the measured signal (S) and the number (N) of atoms responsible for it (this is valid in the single core-loss domain for specimen thickness, *i.e.* up to several micrometres):

$$S = I_0 N \sigma, \tag{4.3.4.49}$$

where I_0 is the incident-beam intensity and σ the relevant excitation cross section in the experimental conditions used, and N is the number of atoms per unit area of specimen. As a satisfactory approximation for taking into account multiple scattering events (either elastic or inelastic in the low-loss region), Egerton (1978) has proposed that equation (4.3.4.49) be rewritten:

$$S(\beta, \Delta) = I_0(\beta, \Delta) N \sigma(\beta, \Delta), \tag{4.3.4.50}$$

where all quantities correspond to a limited angle of collection β and to a limited integration window Δ (eV) above threshold for signal measurement.

A major problem is the evaluation of the signal itself after background subtraction. The method generally used, demonstrated in Fig. 4.3.4.31, involves extrapolating a modelized background profile below the core loss of interest. Following Egerton (1978), the choice of a power law $B(\Delta E) = A \Delta E^{-R}$ is satisfactory in many cases, and the signal is then defined as

$$S(\Delta) = \int_{E_c}^{E_c+\Delta} [I(\Delta E) - B(\Delta E)] \, \mathrm{d}(\Delta E). \tag{4.3.4.51}$$

Numerical methods have been developed to perform this process with a well controlled analysis of statistical errors (Trebbia, 1988).

In many cases, one is interested in elemental ratios; consequently, the useful formula becomes

$$\frac{N_A}{N_B} = \frac{S_A(\beta, \Delta)}{S_B(\beta, \Delta)} \frac{\sigma_B(\beta, \Delta)}{\sigma_A(\beta, \Delta)}. \tag{4.3.4.52}$$

This can be used to determine the N_A/N_B ratio without standards, if the cross-section ratio σ_B/σ_A (also called the k_{AB} factor) is previously known: accuracy at present is limited to ±5% for most edges. But it is also possible to extract from this formula the cross-section (or k factor) experimental values for comparison with the calculated ones, if the local stoichiometry of the specimen is satisfactorily known [Hofer, Golob & Brunegger (1988) and Manoubi *et al.* (1989) for the $M_{4,5}$ edges].

Improvements have recently been made in order to reduce the different sources of errors. For medium-thickness specimens (*i.e.* for $t \simeq \lambda_p$ where λ_P is the mean free path for plasmon excitation), deconvolution techniques are introduced for a safer determination of the signal. When the background extrapolation method cannot be used, *i.e.* when edges overlap noticeably, new approaches (such as illustrated in Fig. 4.3.4.25) try to determine the best simulated profile over the whole energy-loss range of interest. It requires several contributions, either deduced from previous measurements on standard (Shuman & Somlyo, 1987; Leapman & Swyt, 1988), or from reasonable mathematical models with different contributions for dealing with transitions towards bound states or continuum states (Manoubi, Tence, Walls & Colliex, 1990).

(*b*) *Detection limits*

This method has been shown to be the most successful of all EM techniques in terms of ultimate mass sensitivity and associated spatial resolution. This is due to the strong probability of excitation for the signals of interest (primary ionization event) and to the good localization of the characteristic even within the irradiated volume of material. Variations in composition have been recorded at a subnanometre level (Scheinfein & Isaacson, 1986; Colliex, 1985; Colliex, Maurice & Ugarte, 1989). In terms of ultimate sensitivity (minimum number of identified atoms), the range of a few tens of atoms (~10^{-21} g) has been reached as early as about 15 years ago in the pioneering work of

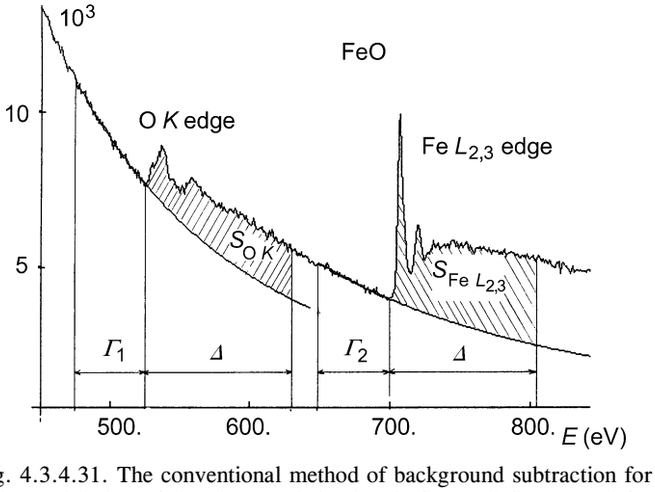

Fig. 4.3.4.31. The conventional method of background subtraction for the evalulation of the characteristic signals $S_{O\,K}$ and $S_{Fe\,L_{2,3}}$ used for quantitative elemental analysis (to be compared with the approach described in Fig. 4.3.4.25).

Isaacson & Johnson (1975). Very recently, a level close to the single-atom identification has been demonstrated (Mory & Colliex, 1989). A major obstacle is then often radiation damage, and consequent specimen modification induced by the very intense primary dose required for obtaining sufficient SNR values.

On the other hand, the EELS technique has long been less fruitful for investigating low concentrations of impurities within a matrix. This is a consequence of the very high intrinsic background under the edges of interest: in most applications, the atomic concentration detection limit was in the range 10^{-3} to 10^{-2}. The introduction of satisfactory methods for processing the systematic sources of noise in spectra acquired with parallel detection devices (Shuman & Kruit, 1985) has greatly modified this situation. One can now take full benefit from the very high number of counts thus recorded within a reasonable time (10^6 to 10^7 counts per channel) and detection of calcium of the order of 10^{-5} atomic concentration in an organic matrix has been demonstrated by Shuman & Somlyo (1987).

(*c*) *Crystallographic information in EELS*

Although not particularly suited to solving crystal-structure problems, EELS carries structural information at different levels:

In a crystalline specimen, one detects orientation effects on the intensity of core-loss edges. This is a consequence of the channelling of the Bloch standing waves as a function of the crystal orientation This observation requires well collimated angular conditions and inelastic localization better than the lattice spacing responsible for elastic diffraction. When these criteria apply, the changes in core-loss excitations with crystallographic orientation can be used to determine the crystallographic site of specific atoms (Tafto & Krivanek, 1982). An equivalent method, known as ALCHEMI (atom location by channelling enhanced microanalysis), which involves measuring the change of X-ray production as a function of crystal orientation, has been applied to the determination of the preferential site for substitutional impurities in many crystals (Spence & Tafto, 1983).

Energy-filtered electron-diffraction patterns of core-loss edges could reveal the symmetry of the local coordination of selected atomic species rather than the symmetry of the crystal as a whole. This type of information should be compared with ELNES data (Spence, 1981).

At large scattering angles, and for energy losses far beyond the excitation threshold, the Bethe ridge [or electron Compton profile (see §§4.3.4.3.3 and 4.3.4.4.2)] constitutes a major feature easily observable in energy-filtered diffraction patterns (Reimer & Rennekamp, 1989). The width of this feature is associated with the momentum distribution of the excited electrons (Williams & Bourdillon, 1982). Quantitative analysis of the data is similar to the Fourier method for EXELFS oscillations. After subtracting the background contribution, the spectrum is converted into momentum space and Fourier transformed to obtain the reciprocal form factor $B(r)$: it is the autocorrelation of the ground-state wavefunction in a direction specified by the scattering vector $\mathbf{q}$. This technique of data analysis to study electron momentum densities is directly developed from high-energy photon-scattering experiments (Williams, Sparrow & Egerton, 1984).

4.3.4.5. *Conclusions*

Since the early work of Hillier & Baker (1944), EELS spectroscopy has established itself as a prominent technique for investigating various aspects of the electronic structure of solids, As a fundamental application, it is now possible to construct a self-consistent set of data for a substance by combination of optical or energy-loss functions over a wide spectral range (Altarelli & Smith, 1974; Shiles, Sazaki, Inokuti & Smith, 1980: Hagemann, Gudat & Kunz, 1975). Sum-rule tests provide useful guidance in selecting the best values from the available measurements. The Thomas–Reiche–Kuhn *f*-sum rule can be expressed in a number of equivalent forms, which all require the knowledge of a function $[\varepsilon_2, \kappa, \mathrm{Im}(-1/\varepsilon)]$ describing dissipative processes over all frequencies:

$$\left.\begin{aligned} \int_0^\infty \omega\varepsilon_2(\omega)\,\mathrm{d}\omega &= \frac{\pi}{2}\omega_p^2, \\ \int_0^\infty \omega\kappa(\omega)\,\mathrm{d}\omega &= \frac{\pi}{4}\omega_p^2, \\ \int_0^\infty \omega\left(-\frac{1}{\varepsilon(\omega)}\right)\mathrm{d}\omega &= \frac{\pi}{2}\omega_p^2. \end{aligned}\right\} \tag{4.3.4.53}$$

One defines the effective number density n_{eff} of electrons contributing to these various absorption processes at an energy $\hbar\omega$ by the partial *f* sums:

$$\left.\begin{aligned} n_{\mathrm{eff}}(\omega)|_{\varepsilon_2} &= \frac{m_0}{2\pi^2 e^2}\int_0^\omega \omega'\varepsilon_2(\omega')\,\mathrm{d}\omega', \\ n_{\mathrm{eff}}(\omega)|_{\kappa} &= \frac{m_0}{\pi^2 e^2}\int_0^\omega \omega'\kappa(\omega')\,\mathrm{d}\omega', \\ n_{\mathrm{eff}}(\omega)|_{-1/\varepsilon} &= \frac{m_0}{2\pi^2 e^2}\int_0^\omega \omega'\left[-\frac{1}{\varepsilon(\omega')}\right]\mathrm{d}\omega'. \end{aligned}\right\} \tag{4.3.4.54}$$

As an example, the values of $n_{\mathrm{eff}}(\omega)$ from the infrared to beyond the *K*-shell excitation energy for metallic aluminium are shown in Fig. 4.3.4.32. In this case, the conduction and core-electron contributions are well separated. One sees that the excitation of conduction electrons is virtually completed above the plasmon resonance only, but the different behaviour of the integrands below this value is a consequence of the fact that they describe different properties of matter: $\varepsilon_2(\omega)$ is a measure of the rate of energy dissipation from an electromagnetic wave, $\kappa(\omega)$ describes

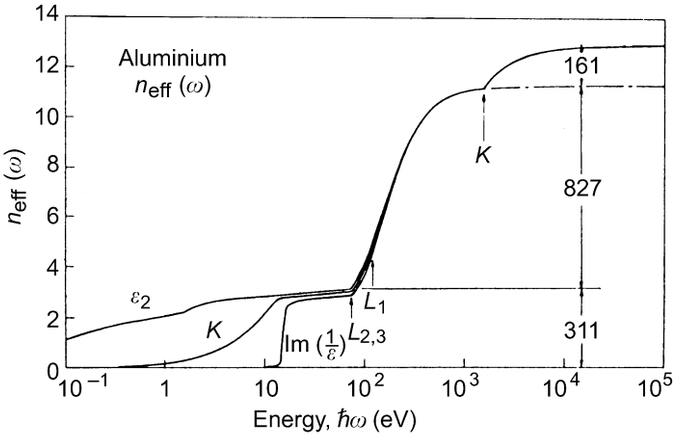

Fig. 4.3.4.32. Values of n_{eff} for metallic aluminium based on composite optical data [courtesy of Shiles *et al.* (1980)].

references